

1 Imaging General

1.1 Plane Waves

$f(\vec{r}, t) = A_0 \cdot e^{j(\vec{k} \cdot \vec{r} - \omega t + \phi)}$ \vec{k} points in the direction of the wave and is orthogonal to the wavefront. $k_x \Delta x + k_y \Delta y = 2\pi$, $\lambda = 2\pi |\vec{k}|^{-1}$

1.2 Resolution

1.2.1 Spatial Resolution: Image(\vec{r}) = Object * PSF (\vec{r}) $\Rightarrow \mathcal{F}\{\text{Im}\}(\vec{k}) = \mathcal{F}\{\text{Ob}\}(\vec{k}) \cdot \text{MTF}(\vec{k})$

MTF describes attenuation of different spatial frequencies. Ideally constant (\Leftrightarrow PSF = δ), in reality Gaussian. SNR = Image intensity/std(intensity)

1.2.2 Contrast: $C = (I - I_{\text{background}}) / I_{\text{background}}$

Scattering reduces contrast: $C^{\text{sc}} = \frac{(I + I_{\text{sc}}) - (I_{\text{bg}} + I_{\text{sc}})}{I_{\text{bg}} + I_{\text{sc}}} = C \frac{1}{1 + I_{\text{sc}}/I_{\text{bg}}}$

Contrast in CT context: $C \propto (\mu_1 - \mu_2)d$

1.2.3 Partial Volume Effect: Happens because of insufficient # of pixels covering the object, i.e. object smaller than $2 \times \text{FWHM}$ resolution. \Rightarrow underestimation of signal. Must not draw boundary of ROI too close to a tissue border.

1.3 Fourier

Gauss \leftrightarrow Gauss: $\sqrt{\frac{2\sigma^2}{\pi}} e^{-\sigma^2 t^2/2} \leftrightarrow e^{-\omega^2/2\sigma^2}$

Const. \leftrightarrow Dirac Delta; White Noise \leftrightarrow White Noise

Comb \leftrightarrow Comb: $\sum_n \delta(t - n\Delta t) \leftrightarrow \sum_n \delta(\omega - n\Delta\omega)$, $\Delta\omega = 2\pi/\Delta t$

Exp \leftrightarrow Lorentz: $e^{-|t|/T_2} \leftrightarrow \frac{2R_2}{(\omega^2 + R_2^2)}$

Sinc \leftrightarrow Rectangle: $2\omega_c \text{sinc}(\omega_c t) \leftrightarrow \chi_{[-\omega_c, \omega_c]}(\omega)$

1.3.1 Projection Slice Theorem: FT of projection of 2D object is equal to slice through origin at same angle in 2D FT of whole object.

1.4 Linear Shift Invariant Systems

Different features should be imaged independently \rightarrow Linear ($S[\alpha f_1 + f_2] = \alpha S[f_1] + S[f_2]$). Depiction of a feature should not depend of position \rightarrow Shift Invariant. Complex exponentials (plane waves) are eigenfunctions $S[f] = S[f](0,0) \cdot f$ for $f(x,y) = e^{i(k_x x + k_y y)}$, where the eigenvalue is the transfer function $H(k_x, k_y)$.

1.4.1 Fourier of LSI: $\mathcal{F}\{S[f]\} = H(k_x, k_y) \cdot \mathcal{F}\{f\}(k_x, k_y) \Rightarrow S[f] = \mathcal{F}^{-1}\{H\} * f \Rightarrow \text{PSF} = \mathcal{F}^{-1}\{H\}$

1.5 Sampling Theorem

To prevent overlapping aliases: $\frac{2\pi}{\Delta x} > \text{BW} \Leftrightarrow \Delta x < \frac{2\pi}{\text{BW}} = \frac{1}{2f_{\text{max}}}$. For sampling k-space: $\Delta k < \frac{2\pi}{\text{FOV}} \Rightarrow$ sampling range \leftrightarrow resolution

1.6 Noise

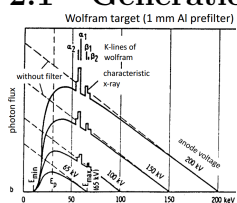
Gaussian: when many independent mechanisms superimpose $P_n(\eta) =$

$\frac{1}{\sqrt{2\pi\sigma^2}} e^{-\frac{\eta^2}{2\sigma^2}}$, **Poisson:** when noise is related to discrete events

$P_n(N) = \frac{\sigma^{2N}}{N!} e^{-\sigma^2}$, SNR: $\frac{|S[f](x,y)|}{\sigma_n}$

2 X-Ray

2.1 Generation $\lambda = 10\text{pm} - 10\text{nm}$



2.1.1 Bremsstrahlung: Fast electron is deflected and slowed by nucleus, accelerated charge emits photon. Continuous spectrum. Interaction depends on Z of nucleus and E_e . $E_{\gamma, \text{max}} = E_e$

2.1.2 Characteristic Radiation: Electron ejects K-shell e^- ($E_e > E_{\text{binding}, K}$), hole is refilled by L-shell or M-shell e^- . Discrete energy peaks $E_{\gamma} = \hbar\omega = E_{\text{binding}, K} - E_{\text{binding}, L}$

2.1.3 Heat Production: Power absorption: $\alpha = \frac{P_{\text{absorbed}}}{P_{\text{incident}}}$, Stefan-Boltzmann law: $W = \sigma(T^4 - T_{\text{env}}^4)$ ($\sigma = 5.7e-12 \frac{\text{W}}{\text{cm}^2 \text{K}^4}$), Wien's displacement law: $\lambda_{\text{peak}} = \frac{b}{T}$ ($b = 2.9e-3 \text{mK}$)

2.2 Attenuation

= Absorption + Scatter = Photoeffect + Compton Scattering

2.2.1 Photoeffect: Is what provides contrast. γ is fully absorbed, knocking e^- out of shell \Rightarrow ionizing! Hole refilled \Rightarrow low keV characteristic X-ray. Probability: $P_{\text{pe}} \propto \rho \frac{Z_{\text{eff}}^3}{E_{\gamma}^3}$ with tissue density ρ and $Z_{\text{eff}} = 7.4(\text{tissue})$, $6.9(\text{lipid})$, $13.8(\text{bone})$. \Rightarrow mostly effective in contrast agent, lead, bone.

2.2.2 Compton Effect: γ scattered off e^- , which recoils. Remaining E depends on scattering angle θ : $\Delta\lambda = \frac{h}{m_e c} (1 - \cos\theta) \Rightarrow E'_{\gamma} = E_{\gamma} / (1 + (\frac{E_{\gamma}}{m_e c^2}) (1 - \cos\theta))$. Probability: $P \propto \rho / E_{\gamma}$

2.2.3 Attenuation Coefficient μ : Exponential decay const.: $N_{\gamma}(d) = N_{\gamma,0} e^{-\mu(E)d}$. Mass attenuation coefficient $\mu' = \mu/\rho$

2.2.4 Beer Lambert's law: $I = \int_0^{E_{\text{max}}} I_0(E) e^{-\int_{-\infty}^{\infty} \mu(E,x) dx} dE$

2.2.5 Pre-Filtering: Low-energy photons only contribute to dose, not image (absorbed). Filter after generation. (1-3mm Al)

2.3 Projection Imaging

2.3.1 Anti-Scatter Grid: Lead lamellae block scattered light. Increases contrast, decreases SNR. Grid ratio = $\frac{h}{d} \in [4, 16]$, grid freq. = $\frac{1}{d-t} \in [5, 7] \text{mm}^{-1}$, with h =lamella height, d =spacing, t =thickness. Bucky factor BF = $I_{0, \text{w/grid}} / I_{0, \text{w/o grid}}$, sodass I_{detected} identisch. BF $\in [4, 10]$.

2.3.2 X-Ray Film: Carrier sandwiched by film (Silver Halide AgX) sandwiched between fluorescent screens (increase efficiency $\times 5$, decrease resolution). $\text{AgBr} \rightleftharpoons \text{Ag}^+ + \text{Br}^-$, $\text{Br}^- + E_{\gamma} \rightarrow \text{Br} + e^-$, $e^- + \text{Ag}^+ \rightarrow \text{Ag} \rightarrow$ washed out.

2.3.3 Computed Radiography: Detector plate from BaFX:Eu $^{2+}$, illumination with x-ray liberates e^- from valence \rightarrow conduction band, e^- trapped. Scanning with laser stimulates decay of trapped e^- back down under emission of blue light \rightarrow detected.

2.3.4 Digital Radiography: For indirect conversion: x-ray \rightarrow CsI:Tl scintillator (rod-like structur, good lightguide, emits green, 0.6mm) \rightarrow photodiode array (TFT).

2.3.5 SNR: Distribution of X-rays per unit area follows Poisson statistics: $P(N) = \frac{\mu^N e^{-\mu}}{N!}$ with $\sigma = \sqrt{\mu}$ and thus SNR=Signal/Noise= $\sqrt{N} \Rightarrow \text{SNR} \propto 1/\sqrt{I_A \cdot t \cdot \Delta z}$ and more complicated dependence on kVp, patient size, anti-scatter grid, detector ϵ and voxel size

2.3.6 CNR: depends on x-ray spectrum (low kVp: photoel.abs. dominates, μ_{bone} and μ_{tissue} very different \Rightarrow high CNR, but low $E \Leftrightarrow$ low SNR), FOV (bigger \Rightarrow more scattering \Rightarrow lower CNR), body thickness (thick \Rightarrow more scattering), anti-scatter grid.

2.4 Contrast Agents

2.4.1 GI Tract: Barium, K-line@37.4keV, administered as suspension of Bariumsulfate powder in water.

2.4.2 IV: Iodine, K-edge@33.2keV, $Z=53$, benzene ring with I at three C's, $R_{1,2,3}$ (determining pharmacokinetics) at others.

2.4.3 Digital Subtraction Angiography: Take image w/o contrast agent, second image w/ agent. Difference = vasculature.

2.5 CT

2.5.1 CT tissue numbers: $\text{CT}_0 = 1000 \text{HU} \cdot (\mu_0 - \mu_{\text{H}_2\text{O}}) / \mu_{\text{H}_2\text{O}}$

Bone:1000..3000, muscle:10..40, water:0, lipid:-50..-100,

Air:-1000, WM:20-30, GM:35-45, blood:40

2.5.2 Radon Transform: same as sinogram. $P_{\varphi}(r) = -R[\mu](r, \varphi)$

$= -\iint \mu(x,y) \delta(x \cos \varphi + y \sin \varphi - r) dx dy = -\int \mu(r,s) ds$

$\mathcal{F}_{1D}\{P_{\varphi}(r)\}(u) = -\iint \mu(r,s) e^{iu(x \cos \varphi + y \sin \varphi)} dx dy$

$\mathcal{F}_{2D}\{P_{\varphi}(r)\}(p,q) = -\iint \mu(x,y) e^{-ipx} e^{-iqy} dx dy$

$\Rightarrow \mu(x,y) = -\frac{1}{4\pi^2} \iint \mathcal{F}\{P_{\varphi}\}(p,q) e^{ipx} e^{iqy} dp dq$

2.5.3 Filtered Backprojection: above formula for μ in polar:

$\mu(x,y) = -\frac{1}{4\pi^2} \int_0^{\pi} \mathcal{F}\{P_{\varphi}\}(\varphi, u) e^{-iur} |u| du d\varphi$

Multiplication in spectral domain \leftrightarrow convolution in real space: $\mu(x,y) = \int_0^{\pi} P_{\varphi}(u) * \mathcal{F}^{-1}\{|u|\} du d\varphi$. $\mathcal{F}^{-1}\{|u|\}$ =Ram-Lak filter.

2.5.4 Simple Backprojection: Problem: blurring around edges b/c PSF $\propto |r^{-2}|$ (partial overlap between different projections). Solution: convolve w/ filter, e.g. Ram-Lak $\propto |r^{-2}|$.

2.5.5 Fourier Reconstruction: Problem: After 1D FT, radial arrangement of sample points, high frequencies sparsely sampled, has to be interpolated to cartesian grid for IFT. Limits spatial resolution (high freq., high res.) Have to sample $\pi/2$ times more: $\pi/2 N_{\text{cart}} = N_{\text{radial}}$

2.5.6 Spiral CT: Gantry rotating during table movement, projections taken on spiral. For backprojection: interpolation of data, makes slicing at arbitrary z-position possible.

$P_{\phi}(r,z) = (1-\lambda)P_{\phi}(r,z_j) + \lambda P_{\phi}(r,z_{j+1})$, with $\lambda = \frac{z-z_j}{z_{j+1}-z_j}$

2.5.7 Image Quality: Recorded intensity: $I(x,y,z) \propto O(x,y,z) * \text{PSF}(x,y,z) + \text{noise}$. noise: Quantum noise (photon # fluctuates), Poisson statistics (see 2.3.5). Pixel noise: $\sigma = \left\{ \frac{1}{M-1} \sum_{i=1}^M (I_i - \bar{I})^2 \right\}^{1/2}$

2.5.8 Dosage: Absorbed dose: $E_{\text{deposited}}/m$. Unit 1Gray = 1Gy = 1J/kg. Equivalent dose: biological effect. Unit 1 Sievert = 1Sv = 1J/kg. [eq.dose] = $Q N[\text{abs.dose}(G_{\gamma})]$. $Q = 1(\gamma)$, $5-20(n^0)$, $5(p^+)$, $20(\alpha^{2+})$. $N = 0.12(\text{bone marrow, GI})$, $0.05(\text{bla., bra., kidney, liver})$, $0.01(\text{bone, skin})$. Bg dose 2.5mSv/y, CT 20mSv

3 Nuclear Imaging

3.1 $^{99\text{m}}_{43}\text{Technetium}$

Used in 90% of all planar scinti/SPECT. $\tau_{1/2} = 6\text{h}$. Decays to $^{99\text{g}}_{43}\text{Tc}$ and photon@140keV.

3.1.1 Production: Parent nuclide $^{99}_{42}\text{Mo}$ from neutron-irradiated uranium targets. $\tau_{1/2} = 66\text{h}$. Shipped in $^{99\text{m}}\text{Tc}$ -generators (moly cow). ^{99}Mo bound as MoO_4^{2-} to Al_2O_3 . After decay TcO_4^- pertechnetate, $^{99\text{m}}\text{Tc}$ bound less strongly, washed out as NaTcO_4 . Generator milked every 24h, b/c Radioactivity $Q \propto (e^{-\lambda_{\text{Mo}} t} - e^{-\lambda_{\text{Tc}} t})$ maximal.

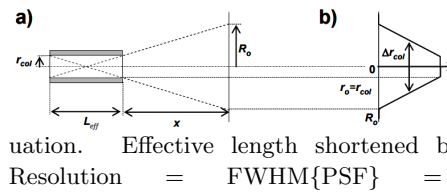
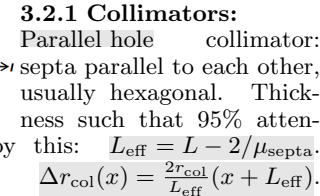
3.1.2 Reaction Kinetics: $^{99}\text{Mo} (N_1) \xrightarrow{\lambda_1} ^{99m}\text{Tc} (N_2) \xrightarrow{\lambda_2} ^{99g}\text{Tc} (N_3)$
 $\lambda_i = \frac{\ln 2}{\tau_{1/2,i}}$. $\frac{dN_2}{dt} = \lambda_1 N_1 - \lambda_2 N_2$. Hom.sol. $N_2 = C e^{-\lambda_2 t}$. Part.sol.
 $N_2 = D e^{-\lambda_1 t}$. $D = \frac{\lambda_1 N_0}{\lambda_2 - \lambda_1}$. Sol.=Hom.+Part. @ $t = 0, N_2 = 0 \Rightarrow 0 =$
 $N_2(0) = C + D \Rightarrow C = -D \Rightarrow N_2 = \frac{\lambda_1 N_0}{\lambda_2 - \lambda_1} (e^{-\lambda_1 t} - e^{-\lambda_2 t})$. $Q_2 = \lambda_2 N_2$

3.1.3 Tc Complexes: Sestamibi enters cells via passive diffusion across plasma + mitochondrial membranes. myocardial Viability marker. Tetrofosmin uptake \propto blood flow rates, reflects tissue viability of heart, muscle, liver, spleen, kidneys

3.1.4 Effective Isotope Halflife: $t_{1/2,\text{eff}} = \frac{t_{1/2} \cdot t_{1/2,\text{bio}}}{t_{1/2} + t_{1/2,\text{bio}}}$

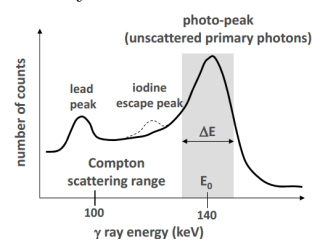
3.2 Gamma Camera

Collimator \rightarrow scinti \rightarrow PMTs \rightarrow PHA and computer.

a)  **b)** 

Resolution = FWHM{PSF} = $\Delta r_{\text{col}}(x) = \frac{2r_{\text{col}}}{L_{\text{eff}}}(x + L_{\text{eff}})$.
 Converging collimator: holes focused towards body, magnifies images, increases spatial resolution. Diverging collimator: larger FOV, lower res., for whole body scinti. Pinhole collimator: very small organs, animals. significant magnification, good res., geometric distortion at image edge. Low SNR. PSF depends on source location and pinhole cone \angle .

3.2.2 Scintillator: NaI:Tl = Thallium activated NaI. γ -ray strikes crystal, loses energy (p.e. and compton) \Rightarrow excited electronic states in crystal. Deexcitation after 230ns \rightarrow blue light @ 415nm, 1 blue γ / 30eV absorbed. NaI:Tl: high $\mu = 2.22\text{cm}^{-1}$ @ 140keV (\rightarrow high Z), high efficiency, transparent to 415nm, grows easily/cheaply, 415nm ideal for PMT, disadv.: hygroscopic. Tradeoff resolution / SNR: Thin crystal = narrow PSF, good res. Thick crystal = many γ detected, high SNR. Usually thickness $\approx 1\text{cm}$. Efficiency $\varepsilon = 1 - e^{-\mu_{\text{crystal}} d_{\text{crystal}}}$



3.2.3 PMT: : Amplitude of signal $\propto E_{\gamma}$. To avoid detection of scattered γ , events binned in MCA and only a range around photopeak are counted. Usually, FWHM of photopeak $\approx 14\text{keV} \approx 10\%$, typically 20% is used. $10^5 - 10^6$ electrons for each incident photoelectron. $\frac{\Delta E}{E_0} = 1/\sqrt{p \cdot N_{\text{ph}}}$, where p =prob. that photoelectron is produced at PMT,

$N_{\text{ph}} = \#$ of photons per γ -photon, $\Delta E = \text{FWHM}\{\text{photopeak}\}$

3.3 Image Quality

3.3.1 SNR: $= \sqrt{\mu}$ (poisson statistics). Tissues deep in body: more attenuation \Rightarrow low SNR. Higher dose \Rightarrow more signal \Rightarrow higher SNR. Collimator properties (eg. longer septa, higher res. but lower SNR). Post acquisition filtering (low pass \Rightarrow higher SNR).

3.4 Resolution

$R_{\text{system}} = \sqrt{R_{\text{gamma}}^2 + R_{\text{coll}}^2} \approx 1\text{-}2\text{cm}(\text{deep}), 5\text{-}8\text{mm}(\text{close})$. R_{col} from collimator, R_{gamma} from uncertainties in camera (accurate pos. of scintillation, error in PMT localization)

3.5 SPECT

Single Photon Emission Computed Tomography. Reconstruction either like CT or iterative process: start with estimate, calculate sinogram, compare with measured sinogram; error acceptable? no: calculate update function, update estimate, start again.

3.6 PET

Positron Emission Tomography. Radionuclide undergoes β^+ decay ($p^+ \rightarrow n + e^+ + \nu$), positron travels a bit until almost resting, then $e^- + e^+ \rightarrow 2\gamma$ @ 511keV each.

3.6.1 Radionuclides: Isotope : $\tau_{1/2}[\text{min}]$: $E_{e^+, \text{max}}[\text{MeV}]$: usage,
 ^{18}F : 110 : 0.63 : onko/inflamm./cardiac viab., ^{11}C : 20.4 : 0.96 : cardiac metab., ^{15}O : 2 : 1.73 : cerebral blood flow, ^{13}N : 10 : 1.2 : cardiac bl.fl., ^{82}Rb : 1.3 : 2.6/3.4 : cardiac perfusion. All except Rb produced in cyclotron, Rb produced from moly-cow like generator. High $E \Rightarrow$ high e^+ range (ultimate resolution limit).

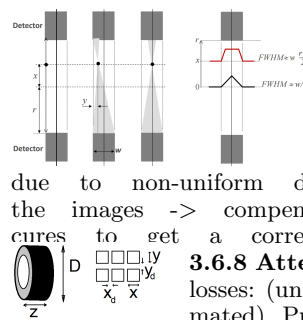
3.6.2 Line Of Response: $r = x \cos \varphi + y \sin \varphi$. There's $\binom{N}{2}$ LORs

3.6.3 Coincidence Detection: Detection in i \Rightarrow signal i set to 1 for t. If during t, detection in j, then sum of two signals goes above threshold and coincidence is counted.

3.6.4 Detector: Segmented block of scinti.mat. (e.g. LSO/BGO ($\mu=0.96/\text{mm}$)) with reflective mat. in cuts (deeper at edges, shallow in middle). PMTs/APDs below. Position of hit calculated from 4 signals.

3.6.5 FWHM: discrete detector pairs: $\text{FWHM} = w \frac{x+x}{2r}$ depth dep. \downarrow
3.6.6 Efficiency: Detection eff. $\varepsilon = (1 - e^{-\mu d})\Phi$ with μ, d scinti atten./thickness, Φ fraction of events in selected E window. Geometric ef-

ficiency:



Axial geom. coverage $\Omega = 4\pi \sin(\text{atan}(\frac{z}{d}))$

Radial geom. coverage $\varphi = \frac{xy}{(x+x_d)(y+y_d)}$

Total $\eta[\%] = 100\% \cdot \varepsilon^2 \varphi \frac{\Omega}{4\pi}$. ε^2 b/c coincidence.

3.6.7 Normalization Correction:

due to non-uniform detector efficiencies \rightarrow structures in the images \rightarrow compensate for the inverse of those structures to get a corrected image \rightarrow take the difference

3.6.8 Attenuation Correction: Correction for losses: (uniform μ assumed and traveled distance estimated). Prob. for absorption of right γ : $p_{1ij} = e^{-\mu x_{ij}}$, left: $p_{2ij} = e^{-\mu(D_{ij} - x_{ij})}$, coincidence: $p_{ij} = p_{1ij} p_{2ij} = e^{-\mu D_{ij}} \Rightarrow$ attenuation correction: $a_{ij} = p_{ij}^{-1} = e^{\mu D_{ij}}$. In PET/CT based on CT data.

3.6.9 Scatter Correction: Analytical method: Assume scatter distribution varies slowly across medium, use phantom data to correct. Dual energy window:

Change of energy by $E'_{\gamma} = \frac{m_e c^2}{m_e c^2 / E_{\gamma} + 1 - \cos \theta}$. Look at second window below p.e. peak. lower window contains scatter only, p.e. peak window true events and scatter. Projection scale&subtract. Simulation method: reconstruction w/o correction, estimation of correction in second step.

3.6.10 Random Coincidence Correction: Frequency of randoms: $N_R = 2\tau N_1 N_2$, with 2τ =coincidence window, $N_{1,2}$ individual detection rates. No geometrical info, almost uniform across FOV \Rightarrow loss in CNR. Measure $N_{1,2}$ coincidences by disabling the synchronization of the receivers. This gives the background noise which can be subtracted afterwards. Alt. parallel coincidence circuit only rand coinc. subtract.

3.6.11 Detector Dead Time: Components: paralyzable (dead time restarts, crystal 230ns to release e^-) and non-(missed count, PHA). Loss of event counts. $N_{\text{measured}} = N_{\text{true}} e^{-N_{\text{true}} \delta_{\text{dead}}}$. Particularly severe for high activities \rightarrow high countrate.

3.6.12 PHA, MCA: PulseHeightAnalyzer: receives sum contributes from MPTs and rejects scattered γ ; MultipleChannelAnalyzer: A/D conv. digitizes signal and produces pulse-height spectrum (#events/E)

3.6.13 Time of Flight: Time res. $\Delta t \approx 500\text{ps} = 7.5\text{cm}$. Improves spatial confinement, sensitivity. Requires extremely fast scintillators.

3.6.14 3D PET: 3D slice rebinning: Data reduced by rebinning events with azimuth of LOR $\theta \neq 0$ into bins of the average \bar{z} . Side effect: axial misregistration. 3DRP reconstruction of $N \times 2\text{D}$ sinograms at azimuth $\theta = 0$, estimation of missing data for $\theta > 0$, forward projection. \Rightarrow better statistics and thus SNR.

3.6.15 Filtering: As high spatial frequencies are sparsely sampled, white noise stronger than signal there. Have to use filters to get rid of noise. Shepp-Logan(M)/Ramp enhance fine-structure, but also noise. Hann (lower M) decreases noise, but also resolution.

3.7 Quantitative PET

3.7.1 ^{11}C : $^{14}\text{N} + p \rightarrow ^{15}\text{O} \xrightarrow{1s} (\alpha) + ^{11}\text{C} \xrightarrow{20\text{min}} ^{11}\text{B} + e^+ + \nu_e$ Proton from cyclotron. Advantages: In principle, all organic compounds can be labelled. Receptor affinity and Pharmacokinetic properties same as cold version \Rightarrow ideal for drug testing. Disadvantages: chemical synthesis difficult (time, need hot cells and synthesis modules). Exposure maybe to short for enrichment at receptor \Rightarrow low target to background.

3.7.2 ^{18}F : $t_{1/2} = 110\text{min}$. Advantages: Half life long enough for synthesis and shipping. Still relatively short study repetition time possible. Disadvantage: Pharmacokinetics different from parent compound unless already fluorinated.

3.7.3 Injected Dose: $\%ID/g = \frac{c_t v_t}{D_{\text{inj}} m_t} \cdot 100\%$ with c_t, v_t, m_t tissue concentration, volume, mass and D_{inj} injected dose.

3.7.4 Stand. Uptake Value: $\text{SUV} = [\%ID/g] / 100\% \cdot M, S$ with either M total body mass or S total body surface. ($< 1\%$ typ.)

3.7.5 Receptor Binding: $L + R \rightleftharpoons RL$. Equilibrium const. $K_d = \frac{k_{\text{off}}}{k_{\text{on}}} = \frac{[L][R]}{[RL]}$. Principle of microreversability $k_{\text{off}}[RL] = k_{\text{on}}[R][L]$. Mass conservation $[R_T] = [R] + [RL]$. Put this in eq. const.: $\frac{[RL]}{[L]} = -\frac{1}{K_d}[RL] + \frac{[R_T]}{K_d}$ (Scatchard equation). For $[RL] \ll [R_T]$: $\frac{[RL]}{[L]} = \frac{[R_T]}{K_d} = \frac{B_{\text{max}}}{K_d}$ (with B_{max} the max binding capacity)

3.7.6 Tracer Extraction: Extraction factor $E = 1 - e^{-P \cdot S/F}$ with capillary permeability P , cap. surface S , flow F . (Renkin-Crone).

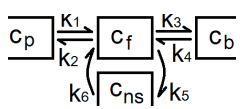
3.7.7 Distribution Volume: $V_d = \frac{M}{c_{bl}}$ with total amount of tracer M and measured concentration in blood c_{bl} . Very high: tracer lipophilic, around 70L: tracer goes to lean body mass, around 5L: tracer stays in blood.

3.7.8 Partition coefficient: $\lambda = \frac{c_t}{c_{bl}}$ with tissue concentr. c_t

3.7.9 Distribution in Tissue Compartments: 4 compartment model can be simplified to 3 comp. by assuming k_5 and k_6 to be fast in comparison to the other rate constants. p: plasma, f: free (in tissue), ns: non-specific bound, b: bound.

For instant equilibration: $c_f = f_2 \cdot (c_f + c_{ns})$ with $f_2 = k_6/(k_5 + k_6)$ and $c_f = k_1 c_p - (k_2 + k_3) c_f + k_4 c_b$, $\dot{c}_b = k_3 c_f - k_4 c_b$. $k_1 = F \cdot E$, $k_2 = k_1 \frac{c_p}{c_f}$ (diff.outflow), $k_3 = k_{on}[R]$, $k_4 = k_{off}$. Solution:

$$\alpha_{1,2} = \frac{1}{2} \{k_2 + k_3 + k_4 \pm ((k_2 + k_3 + k_4)^2 - 4k_2 k_4)^{1/2}\}, a_i = \frac{k_3 + k_4 - \alpha_i}{\alpha_2 - \alpha_1}$$

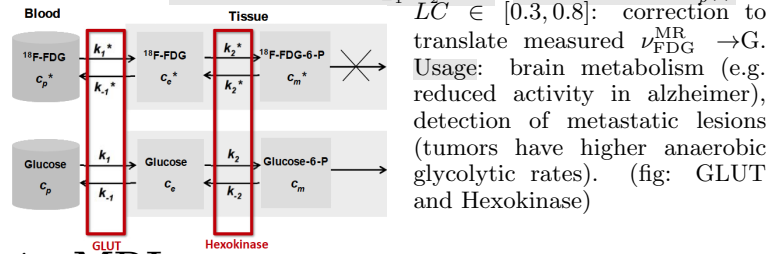


$c_t(t) = c_f + c_b = k_1 \sum_{i=1}^2 a_i e^{-\alpha_i t} * c_p(t)$, w/o receptor $c_t(t) = c_f(t) = k_1 e^{-k_2 t} * c_p(t)$.
3.7.10 Competition Between Hot and Cold Drug: $[R_T] = B_{max} = c_b^*(t) + c_b(t) + B'_{max} \approx c_b(t) + B'_{max}$. Receptor occupancy for cold drug: $RO = \frac{c_b}{B_{max}} \cdot 100\% = (1 - \frac{B'_{max}}{B_{max}}) \cdot 100\%$. Assumptions: Same # of receptors available for hot/cold ligands; Dose linearity: $\Leftrightarrow \frac{B_{max}}{c_b^*} = \frac{B'_{max}}{c_b^*}$. Plotting $c_t(t)$, we would expect it high for compartment expressing receptor and low for not-expressing receptor (after build-up).

3.7.11 Drug Testing: To measure behaviour of a drug (cold ligand): Make tracer (hot ligand) that goes to the same receptors. Do experiment with ($\rightarrow B'_{max}$) and without drug ($\rightarrow B_{max}$). The drug changes the # of total receptors from B_{max} to B'_{max} . E.g. for dopaminergic system in cerebral cortex: apply $[^{11}C]$ raclopride, binds to D2 receptors. Scan. Administer drug, displaces tracer. Scan. \rightarrow determine selectivity of drug, occupancy of receptor. Similar for serotonin (5HT) with 5HT₂ receptor. \Rightarrow FDG6P trapped in cell.

3.7.12 Glucose Metabolism: Measured with $[^{18}F]$ -2-fluoro-2-deoxyglucose (FDG). Taken up from plasma

into cell ($c_p^* \xrightarrow{k_1^*} c_e^*$). Phosphorylated by hexokinase (k_2^*) like glucose (G), but not further by isomerase to fructose. Metabolic rates FDG/G: $\nu_{FDG}^{MR} = k_2^* c_e^*(t) \approx \frac{k_1^* k_2^*}{k_{-1}^* + k_2^*} c_p^*(t)$. $\nu_G^{MR} \approx \frac{1}{LC} \nu_{FDG}^{MR} \frac{c_p(t)}{c_p^*(t)}$.



4 MRI

Magnetic moment $\vec{\mu} = \gamma \vec{S}$ with gyromagnetic ratio γ ($\mu_z = \pm \gamma \hbar / 2$). $\frac{\gamma}{2\pi}$ in MHz/T: $^1H=42.6$, $^{13}C=10.71$, $^{19}F=40.07$, $^{31}P=17.24$

Energy of spin in $\vec{B}||\hat{z}$: $E = -\vec{\mu} \cdot \vec{S} = -\mu_z B_0 = \pm \frac{\hbar}{2} \gamma B_0$. Population of up/down states follows Boltzmann statistics: $\frac{n_{down}}{n_{up}} = e^{-\Delta E / k_B T}$.

$\Delta E = \hbar \omega_L$ To facilitate transitions irradiate at Larmor frequency: $\omega_L = \gamma B_0$. Net magnetic moment: $\vec{M}_0 = \sum \mu_i = \Delta n \mu_z$, $\frac{\Delta n}{n} = \frac{\gamma \hbar B_0}{2 k_B T}$

tissue: T1 @ 1.5T : T1 @ 0.5T : T2 [ms], WM : 790 : 539 : 92, GM : 920 : 656 : 100, CSF : >2500 : >2500 : >2000, Skeletal muscle : 870 : 600 : 47, Liver : 490 : 320 : 40, Fat : 260 : 215 : 85

4.1 Bloch Equations

$$\frac{d}{dt} \vec{M} = \begin{pmatrix} -1/T_2 & -\gamma B_z & \gamma B_y \\ \gamma B_z & -1/T_2 & -\gamma B_x \\ -\gamma B_y & \gamma B_x & -1/T_1 \end{pmatrix} \vec{M} + \begin{pmatrix} 0 \\ 0 \\ M_0/T_1 \end{pmatrix}$$

with $\omega = \gamma |B|$, spin-spin relaxation (transverse components decay with $R_2 = 1/T_2$), spin-lattice relaxation (z-component returns to M_0 with $R_1 = 1/T_1$). Transverse component effectively decays faster because of phase coherence loss (b/c inhomogeneities in B_0). $T_2^* = (1/T_2^2 + 1/T_2)^{-1}$ $M_z(t) = M_0 - M_0(1 - \cos(\alpha))(1 - \exp(-t/T_1))$ $M_y(t) = M_0 \sin(\alpha) \exp(-t/T_2)$

4.1.1 Magnetisation Manipulation: Apply external B -field rotating in xy at Larmor frequency: $B_{x,y} = B_1 \cos, \sin(\omega_L t)$. Tip angle $\alpha = \gamma B_1 \tau_{B1}$. Signal is maximized at the Ernst angle: $\alpha_E = \arccos(e^{-T_R/T_1})$. In rotating frame, \vec{M} then rotates around \vec{B}_1 with $\omega = \gamma B_1$. (Assuming $t_{excitation} \ll T_{1,2}$); correction: $B_z = B_0 - \omega_{RF}/\gamma$.

4.1.2 Detection of Precession: Faraday: $\oint_{\partial S} \vec{E}(\vec{r}, t) d\vec{r} = -\frac{d}{dt} \iint_S \vec{B}(\vec{r}, t) d\vec{\sigma}$. Use with conductive loop. Rotating magnetisation in volume V at \vec{r}_0 generates magnetic field $\vec{B}(\vec{r}, t) = \hat{B}(\vec{r}) e^{i\omega t}$

which induces $\hat{U}_{ind} = i\omega \int_{coil} \hat{B}(\vec{r}) d\vec{A}$. For transmit field $\hat{B}^t(\vec{r}_0)$ driven with I_0 , $U_{ind} = i\omega I_0^{-1} \hat{\mu} \cdot \hat{B}^t(\vec{r}_0)$. With $\vec{\mu} = V(M_{xy}, -iM_{xy}, 0)^T$, we have $U_{ind} = M_{xy} V i\omega B_1^{(-)}$ and coil sensitivity $s(\vec{r}) = i\omega B_1^{(-)}$ with

$$B_1^{(-)} = I_0^{-1} (\hat{B}_x^t(\vec{r}) - i\hat{B}_y^t(\vec{r})).$$

Circular current: $\vec{B}(\vec{r}) = \frac{\mu_0 I}{4\pi} \oint_C \frac{d\vec{l} \times (\vec{r} - \vec{r}')}{|\vec{r} - \vec{r}'|^3}$ (Biot-Savart), works well for low freq./quasi stationary approx., for sample size $\ll \lambda$ ($@7T: \lambda=13cm$). $\uparrow D_{coil} \rightarrow$ Depth \uparrow Sensitivity \downarrow

4.1.3 Free Induction Decay: After turning off B_1 , signals in x and y are oscillation enveloped by exponential decay. Spectrum = Lorentz peaks from water and lipid (lower freq.) with $FWHM = 1/(\pi \cdot T_2^*)$.

4.2 Noise

4.2.1 Resistor Voltage Noise: $\sigma_{noise}^2 = 4k_B T R BW$ (Johnson, Nyquist). Equivalent R of sample: Current I_0 generates field \vec{E} , dissipated power $P = \iiint \sigma(\vec{r}) |\vec{E}(\vec{r})|^2 dV \Rightarrow R = \frac{P}{I_0^2}$. J.N.

assumes constant R across BW (but receiver coil is tuned circuit) and T across setup (but 310K for body, 77K+ for coil). Eff. R: $R_{sample}^{eff} = \frac{1}{2\pi BW} \int_{sample} \int_{\omega_1}^{\omega_2} \frac{\sigma(\omega, \vec{r}) |\vec{E}(\omega, \vec{r})|^2}{I_0^2} d\omega dV \Rightarrow \sigma_{noise}^2 = 4k_B BW (R_{sample}^{eff} T_{sample} + R_{coil}^{eff} T_{coil} + R_{env}^{eff} T_{env})$. Reducing noise: Reduce BW (but longer scan time), T (impractical) or R (copper/silver for coil, cool). Effects of magnetic field negligible (true for biol. samples). Sources are: electric charges and dipoles.

$$\text{4.2.2 SNR: } = \frac{U_{signal}}{\sigma(U_{noise})} = \frac{\omega B_1^{(-1)}(\vec{r}) M_{xy}(\vec{r}) \Delta V}{\sqrt{4k_B BW (T_{sample} R_{sample} + T_{coil} R_{coil})}} \sqrt{N_{avg}}$$

SNR $\propto \Delta V \sqrt{t_{scan}}$. Increasing SNR: Signal side: increase $B_1^{(-1)}(\vec{r})$ (e.g. smaller TX coil), increase magnetization $M_{xy}(\vec{r}) \propto B_0$, increase frequency $\omega \propto B_0$. Noise side: above.

4.2.3 Resolution: Relaxation limit: If data acq. long relax. $H(k) = \text{rect}(\frac{k}{2k_{max}}) e^{-\frac{k^2}{T_2^2}} \Rightarrow$ (FT = sinc*Lorentz) $\Delta x \geq FWHM = \frac{\pi}{\gamma G_{max} T_2^*}$

Sol. $t_{scan} \downarrow$ G \uparrow . Diffusion limit: $\langle \Delta x^2 \rangle = 6DT_{ACQ} \Rightarrow$ (with $D = 10^{-3} \frac{mm^2}{s}$ and $T_{ACQ} = 10ms$) $\Delta x \geq 8\mu m$ eq. valid 4 free diff.

4.3 Image Acquisition

Assuming axial slice with normal in z .

4.3.1 Field Gradients: Maxwell pair in z , Golay pairs in x, y . $G_i = \frac{\partial B_z}{\partial i}$.

4.3.2 Slice Selection: Apply G_z , send in 90° -pulse with bandwidth $\Delta\omega_s$ centered at $\omega_s = \omega_L(z = \text{slice centre})$. Ideal RF-excitation to achieve this frequency profile: $B_1(t) = K \cdot \text{sinc}(\Delta\omega_s \pi t) \cdot \sin(2\pi\omega_s t)$. Slice thickness $T = \frac{2\Delta\omega_s}{\gamma G_z}$. During τ_{grad} (small to avoid M attenuation), different phases accumulate in the slice $\varphi_{slice}(z) = \gamma G_z z \tau_{grad}/2 \rightarrow$ rephasing gradient $G_z^{reph} = \frac{\tau_{grad} G_z}{2\tau_{reph}}$

to avoid signal loss (M). $\varphi_{slice}(z)$ is due to Fourier Slice Theorem: frequency shift \rightarrow phase increases linearly.

4.3.3 Phase Encoding: During time τ_{pe} , G_y is switched on. Spins precess with $\omega(y) = \gamma G_y y + \omega_0$ and acquire different phases $\varphi_{pe}(G_y, \tau_{pe}) = \gamma G_y y \tau_{pe}$.

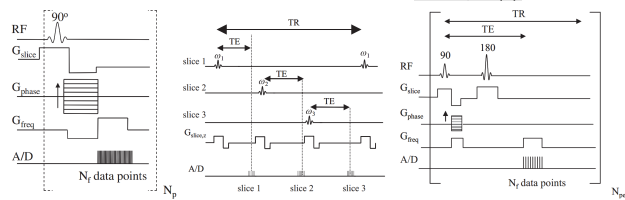
4.3.4 Frequency Encoding: During signal acquisition, G_x is turned on. Spins precess with $\omega(x) = \gamma G_x x + \omega_0$ and thus the spectrum represents a projection of xy onto x . For image with $N_x \times N_y$ pixels, signal is sampled N_x times and whole process is repeated $N_{pe} = N_y$ times with different G_y , taking a total time $T = T_{rep} N_{pe}$ where the repetition time T_{pe} needs to be long enough to allow for sufficient T_1 relaxation.

4.3.5 k-Space Formalism:

Signal: $s(G_y, \tau_{pe}, G_x, t) \propto \iint \rho(x, y) e^{-i\gamma G_y y \tau_{pe}} e^{-i\gamma G_x x t} dx dy$
Spatial frequencies: $k_x = \frac{\gamma}{2\pi} G_x t$, $k_y = \frac{\gamma}{2\pi} G_y \tau_{pe}$
 $\Rightarrow S(k_x, k_y) \propto \iint \rho(x, y) e^{-i2\pi k_x x} e^{-i2\pi k_y y} dx dy = \mathcal{F}\{\rho(x, y)\}$

4.3.6 Object- vs k-Space: Voxel size $\Delta x = \frac{FOV_x}{N_x}$. Sampling distance k-space: $\Delta k_x = \frac{BW_x}{N_x} = \frac{2\pi}{FOV_x}$. Resolution in one space translates to extent in other and vice-versa.

4.3.7 Traversing k-Space speed: $\vec{k} = \gamma \vec{G}(t)$ \vec{G} gives direction



4.3.8 Imaging Sequences: Gradient Echo Imaging: Most basic and fastest. Scan one line of k-space, wait until repetition time over (as $T_2^* \ll T_1$, $TE < TR$), scan next line. Image intensity

$$I(x, y) \propto \rho(x, y) \frac{(1 - e^{-\frac{TR}{T_1}}) \sin \alpha}{1 - e^{-\frac{TR}{T_1}} \cos \alpha} e^{-\frac{TE}{T_2^*}}$$

with the magnetisation angle α . Maximal intensity for given TR for ernst angle.

Multi-slice G.E. imaging: waiting time: $TR - TE \rightarrow$ max # slices: TR/TE . Scan line 1 of slice 1, then immediately l1s2, l1s3, ..., after TR is up l2s1, l2s2, ... or interleaved fashion (even, odd) Spin echo Disadvantage G.E.: cannot weight by T_2 , only $T_2^* \rightarrow$ reverse phase coherence loss with 180° pulse after slice selection, phase encoding and prephasing, then waiting for same time before ACQ. $\vec{k} \rightarrow -\vec{k}$ in the k-space, thus prephasing (go to left of BW) must happen with same gradient sign as during ACQ. Intensity: $I(x, y) \propto \rho(x, y) (1 - e^{-\frac{TR}{T_1}}) e^{-\frac{TE}{T_2^*}}$

Echo Planar Imaging: Scan multiple lines per excitation (after ACQ, go to next line with G_{pe}). Turbo Spin Echo: Same as EPI, but with additional 180° -pulses before each ACQ (T2 weighting \uparrow /suscept. \downarrow)

Inversion Recovery: a SE seq. preceded by 180° RF pulse. Elapsed

time between the 180° and 90°, TI (inversion). We can suppress fat (Short tau IR STIR) or fluid (Fluid attenuation IR, FLAIR, or double IR, DIR). Sh. TI, longer T1 contribute to T2 contrast. Magnitude reconstruction ($|M_z|$ null dark) or phased-sensitive IR (neg M_z dark).

4.3.9 Weighting: Proton Density: $TE \ll T_2^*$ & ($\alpha \ll \alpha_{Ernst}|TR \gg T_1$). T_1 : $TE \ll T_2^*$ & ($\alpha \sim \alpha_{Ernst} | TR \sim T_1$). T_2^* : $TE > T_2^*$ & ($\alpha \ll \alpha_{Ernst}|TR \gg T_1$). mixed T_1 and T_2^* : $TE > T_2^*$ & ($\alpha \sim \alpha_{Ernst}|TR \sim T_1$).

4.3.10 MR Angiography: T_1^{eff} of blood smaller, because during TR, new unsaturated blood flows into slice. $T_1^{eff} = (\frac{1}{T_1} + \frac{v_{blood}}{d_{slice}})^{-1}$. Use heavily T_1 -weighted seq (sh. TR and lar. α). $v_b \cdot TR > S_{th} \rightarrow T_1 = 0$

4.3.11 Contrast Agents: Based on Gadolinium ion in chelate. One electron binding site not occupied, which water can temporarily bind to and undergo rapid T_1 relaxation.

4.3.12 fMRI: Blood oxygenation level dependent (BOLD) effect. Neural activity \rightarrow increased blood flow and thus oxygenation. DeoxyHb is paramagnetic (oxyHb diam.), disturbs local m field \Rightarrow shorter T_2^* and broad dist. res. f. Use EPI (short TE) for speed. Changes in intensity only $\approx 0.3\%$, \rightarrow repeat stimulation/baseline several times. Detect active regions in response to stimulus \rightarrow corr. % Bold response

4.3.13 Diffusion Weighted Imaging: Employ 90°, switch on gradient, different phases accumulate. 180°, wait same time. All phases back to 0, except for protons that diffused away from initial location, which decreases signal. **Diffusion Tensor Imaging:** Ellipse to show diffusion direction. Signal depending on diffusion tensor T and gradient \vec{G} : $S(\vec{G}) \propto e^{-b\vec{G}^T \underline{D} \vec{G}}$. b-value: how strong and how long G on (s/mm^2) if \uparrow b, sig \downarrow . depending on measurement parameters. Measure for different \vec{G} , solve for D . Anisotropic diff. we have a preferential direction \rightarrow connectivity map (axons wrapped myelin, hydrophobic). for restricted diff. $R = \sqrt{2 \cdot D \cdot \Delta}$, $D = \lambda \cdot v/6$, λ free path length, v mol. velocity.

4.4 Instrumentation

4.4.1 Magnets: Outermost layer: B_0 magnet, cryogenics. Further in: Gradients (Maxwell and Golay pairs, see above). Innermost: RF body coils (birdcage built into MRI, almost always used for TX, smaller localized coils for RX).

4.4.2 Stray Fields: strongly shielded by shield coils. 5Gauss=0.5mT (kills pacemakers, magnetstrips) ~ 5 m from MRI. 50Gauss (mag.obj. become projectiles) 2m from MRI.

4.4.3 Peripheral Nerve Stim.: gradient fields may cause E field loops (Eddy currents) which give a ΔV across the membrane \rightarrow causes AP. The factor of cardiac nerve stim. is 80-times higher than per.

nerves. Safety limit: $\sqrt{\sum (w \frac{\partial B}{\partial t})^2} < 20 \frac{T}{s} (1 + \frac{0.36ms}{t_s})$

5 Ultrasound

Speed: $c = 1/\sqrt{\kappa\rho}$ P: $p = \rho c u_z$ Impedance: $Z = p/u_z = \rho c = \sqrt{\rho/\kappa}$ Intensity: $I = pu_z/2$ WL: $\lambda = c/\nu = 1/(\nu\sqrt{\kappa\rho})$ Part.vel: $u_z = \sqrt{2I/Z}$

5.1 Some Material Properties

Subst($Z[kg/m^2s]$; $\rho[g/cm^3]$; $c[m/s]$); Water($1.48 \cdot 10^6$; 1.0; 1480); Muscle($1.66 \cdot 10^6$; 1.06; 1568); Bone($6 \cdot 10^6$; 1.3-1.8; 2800-4100); Air(400(!); 0.0012; 330); PZT-5 Ceramic($29 \cdot 10^6$; 7.65; 3790)

5.2 Fresnel Equations

$$R_p = \frac{p_r}{p_i} = \frac{Z_2 \cos \theta_i - Z_1 \cos \theta_t}{Z_2 \cos \theta_i + Z_1 \cos \theta_t} \quad T_p = \frac{p_t}{p_i} = \frac{2Z_2 \cos \theta_i}{Z_2 \cos \theta_i + Z_1 \cos \theta_t}$$

$$R_I = \frac{I_r}{I_i} = \frac{(Z_2 \cos \theta_i - Z_1 \cos \theta_t)^2}{(Z_2 \cos \theta_i + Z_1 \cos \theta_t)^2} \quad T_I = \frac{I_t}{I_i} = \frac{4Z_1 Z_2 \cos^2 \theta_i}{(Z_2 \cos \theta_i + Z_1 \cos \theta_t)^2}$$

$$T_p = R_p + 1 \quad T_I = 1 - |R_I|^2$$

5.3 Scattering

Rayleigh scattering, if $d \ll \lambda$. Then $E_{scatter} \propto \lambda^{-4}$ and slightly more backscatter than forward. If objects close together, backscatter adds up constructively (\rightarrow Doppler US), if further apart, con/destructive interference leads to speckle (char. wavelength: $\lambda/2$), image has granular appearance; reduced w compound img. clutter signal arises from side/grating lobes reflection, reduced with harmonic img. These 2 reduce SNR/CNR.

5.4 Attenuation

$I(z) = I_0 e^{-\mu z}$ with $\mu [dB/cm] = 4.343 \mu [cm^{-1}]$; $p(z) = p_0 e^{-\alpha z}$ $\mu = 2\alpha$; Material [attenuation in dB/(cm MHz)]: kidney&brain [1.0], liver [0.8-1.3], muscle [1.5-2.2], fat [0.5], bone [13]

5.5 Transducer

Piezo from lead zirconate titanate (PZT). Matching layer with $Z = \sqrt{Z_{PZT} Z_{skin}}$, $d = \lambda_{US}/4$. Damping behind PZT to decrease ringing and allow short pulses (axial res. \propto pulse length), also increases resonator bandwidth.

5.5.1 Beam Geometry: Near-field = Fresnel zone: complicated wave pattern with lots of zeros in intensity, unsuited for diagnostics. Far-field = Fraunhofer zone: intensity decays exponentially. Boundary at $Z_{NFB} \approx r^2/\lambda$ with the transducer radius r . At NFB: beamwidth approx. equal to $2r$, afterwards divergence with $\theta = \arcsin(0.61\lambda/r)$. In far-field, lateral beam shape is Gaussian. Lateral resolution = FWHM = 2.36σ .

Axial resolution $\Delta z = t_{pulse} c/2 = L_{pulse}/2$. Implies $\Delta z \geq \lambda/2$. Typically 1.5mm@1MHz, 0.3mm@5MHz.

5.5.2 Focusing: Focusing by lenses or concave transducer face. Strong focusing \Rightarrow good lateral resolution at focal point, big divergence. Weak focusing \Rightarrow medium lateral resolution, longer focal depth. $f\#$ = focal distance / diameter of transducer. Lateral resolution $\lambda f\#$.

5.5.3 Linear Arrays: 128-256 transducers in flat array. Typical dim: 10-15cm \times 1cm. Pitch (period) $\approx \lambda$. Kerf (spacing of transducers) $\approx 30\mu m$. Operated one to few transducers at a time. Sweep left \rightarrow right. Lateral resolution limited by pitch, but small pitch \Rightarrow small θ .

5.5.4 Phased Array: Smaller and more densely packed transducer. Pitch $< \lambda/2$. Beam focusing and steering happens by phasing the output of different transducer elements. Small aperture and beam steering \Rightarrow looking through acoustic windows possible.

5.5.5 Receiver Beam-Forming: TX and RX with same beam direction and focus. Analog: phased RX signal combination with delay lines, 1 signal recorded. Digital: all channels recorded, combination later.

5.5.6 Beam steering: Steer the beam by ϕ by applying a phase diff of $\Delta\phi = -k y \sin(\alpha)$ to each transducer, y its y-coordinate.

5.5.7 Beam focusing: Focusing is achieved by phasing the array elements such that their partial waves have equal phase at the focus point: $\Delta\phi = -k\sqrt{y^2 + (d/\cos(\alpha))^2 + 2y d \sin(\alpha)/\cos(\alpha)} \approx -k\sqrt{y^2 + d^2}$ with d the focus distance along the x dir.

5.5.8 Multidimensional Arrays: Few rows in elevation direction allows some focusing (1.5D array). Large number of rows allows steering and focusing in both directions (2D array).

5.5.9 Grating Lobes: Channel-to-channel phase increment: $\Delta\phi \bmod 2\pi = kd \sin \alpha$ with $\alpha = \angle(\text{transducer normal, wave propagation})$ and pitch d . \Rightarrow To avoid side lobes ensure $d \leq \lambda/2$

5.6 Time Gain Compensation

Signals arriving later are amplified more strongly, counteracting the exponential attenuation in tissue and reducing dynamic range.

5.7 SNR

$S/N = \text{dyn. range} - \text{attenuation} - \text{loss from reflection}$ [dB] dynamic range [dB] = $10 \log(P_{tx}/P_{noise})$ reflection loss [dB] = $20 \log(\text{loss} [\%])$

5.8 Scanning Modes

5.8.1 A-Mode: Scans only one line. Mainly in ophthalmology.

5.8.2 M-Mode: Records motion by recording A-spectra and plotting them (brightnesscoded) against time.

5.8.3 B-Mode: 2D image by scanning each line as A-mode. Steering electronic for line/phased arrays, mechanical for annular.

5.8.4 Scanning Procedures: Parallel scan for large acoustic windows, sector scan (lines fanning from transducer) for small acoustic window, radial scan for inside of vessels. **Compound scan** acquired from multiple angles by phased array and different beam forming schemes to average out speckle, make boundaries \parallel beam visible and reduce acoustic enhancement/shadowing (after low/high attenuating tissue).

5.9 Doppler Ultrasound

Erythrocytes $\approx 7\mu m$, US $\lambda \approx 0.1\text{-}1\text{mm}$ Observer receives: $f^{eff} = f_i \frac{c+v}{c}$

$$f_{rec} = \frac{f_i(c+v \cos \theta)^2}{c^2} \Rightarrow \Delta f = f_{rec} - f_i \approx \frac{2f_i v \cos \theta}{c} \Rightarrow v = \frac{c \Delta f}{2f_i \cos \theta}$$

with flow velocity v , recorded/initial frequencies $f_{rec,i}$, Winkel $\theta = \angle(\vec{v}, \text{beam})$ (recorded with Bmode prev) Frequency shifts on order of 0.05%, use high frequency so the backscatter is stronger ($\propto \omega^2$), make sure θ small. **CW Doppler:** Used when there's no need to localize source. Half of transducer elements used for transmission, half for reception.

Not limited to maximal depth or flow velocity. Received signal is demodulated with transmission, which shifts spectrum such that $f_i \rightarrow 0$ and $f_i + \Delta f \rightarrow \Delta f$, but also introduces harmonics ($2f_i$ and $2f_i + \Delta f$), filtered out by LPF. Scatter from stationary structures filtered out by HPF. **Quadrature Demodulation:** If demodulation happens with cos only, one gets $|\Delta f|$. To differentiate between positive and negative doppler shift one takes two time-domain multiplication: one with the original transmitter waveform and one with the same waveform shifted by 90° in phase. With the cos and sine one is able to create an exponential \rightarrow a single Dirac peak with a meaningful negative range of the spectrum. **Flow Profiles:** Laminar flow: at lower velocities, flat Doppler spectrum distribution up to $f_{max} \hat{=} v_{max}$. Plug flow: at higher speeds (eg. systole), distinct peak in spectrum. **Time-resolved Frequency Analysis:** Weight continuous signal with \cos^2 -window, perform FFT. **Sonogram:** Color code amplitude, plot freq against time.

Pulsed Doppler: Focus beam to depth of interest d , when transmitter gate on, send pulses at pulse repetition rate $f_{prf} = 1/t_{rep}$, open receiver gate at $t = 2d/c$. In time: signal poulsed by rect \rightarrow sampled sinc in freq. Received signal has stationary part and doppler shifted part. (see demod.) Maximal velocity measurable limited by PRR: $|\Delta f_{max}| = f_{rep}/2 \Rightarrow |v_{max}| = f_{rep} \cdot c/(4f_i)$ (else aliasing and ambiguity in the signal). PRR is limited by depth ROI: $d_{max} = c \cdot t_{rep}/2 = c/2f_{rep}$ = Axial resolution (v_{max} as f_{Dmax} reduced with d). f_{prf} sample freq in F-space. Hence: the higher the pulse freq the lower the spat. res.